

# Rainfall Information System Based on Weather Radar for Debris Flow Disaster Mitigation

Ratih Indri Hapsari<sup>1\*</sup>, Gerard Aponno<sup>1</sup>, Rosa Andrie Asmara<sup>2</sup> Satoru Oishi<sup>3</sup>,

<sup>1</sup> Department of Civil Engineering, State Polytechnic of Malang

<sup>2</sup> Department of Information Technology, State Polytechnic of Malang

<sup>3</sup> Research Center for Urban Safety and Security, Kobe University, Japan

\*Corresponding author E-mail: [ratih@polinema.ac.id](mailto:ratih@polinema.ac.id)

## Abstract

Rainfall-triggered debris flow has caused multiple impacts to the environment. It is regarded as the most severe secondary hazards of volcanic eruption. However, limited access to the active volcano slope restricts the ground rain measurement as well as the direct delivery of risk information. In this study, an integrated information system is proposed for volcanic-related disaster mitigation under the framework of X-Plore/X-band Polarimetric Radar for Prevention of Water Disaster. In the first part, the acquisition and processing of high-resolution X-band dual polarimetric weather/X-MP radar data in real-time scheme for demonstrating the disaster-prone region are described. The second part presents the design of rainfall resource database and extensive maps coverage of predicted hazard information in GIS web-based platform accessible both using internet and offline. The proposed platform would be useful for communicating the disaster risk prediction based on weather radar in operational setting.

**Keywords:** Rainfall, Debris flow, Weather radar, Disaster, WebGIS.

## 1. Introduction

Debris flow disaster triggered by heavy rain is noticed as the most serious secondary impact of volcanic disaster. In aftermath of eruption, the mountain flank is usually difficult to access and the rain observation stations may be damaged during emergency. Weather radar is promising equipment for observing rainfall remotely with high accuracy. Compared to the conventional radar, X-band multiparameter weather radar/X-MP radar provides more fine rainfall information (Kato and Maki, 2009) which is very advantageous for hydrological purpose.

The estimation and prediction of triggering rainfall require detail precipitation monitoring, as the debris flows have small time and spatial scales. For short flooding lead times, rainfall nowcasting is required for forecasting the near future events. Radar echo extrapolation techniques have been the mainstream of rainfall very-short-term prediction (Reyniers, 2008). Distinguishing the hazardous and non-hazardous events in particular sub-basin is necessary for the warning issuance in emergency situation. Rainfall critical line is broadly applied in sediment flow researches and operations (Neary et al., 1987) for determining the triggering rain which causes material movement. However, they were not developed by using the data from weather radar observations.

Disaster risk information is a major element of disaster mitigation system (Bradley et al, 2014). Communicating the rainfall data, particularly the forecast products to the user at the risk-prone area is a challenging part of the risk information. The prime motivation is to assist better decision making for those receiving the information. An attractive prospect is the use of relatively complex graphics with web-based system. X-band Polarimetric Radar for Prevention of Water Disaster (X-Plore) is a platform of infor-

mation system of rainfall monitoring and nowcasting from X-MP radar. In the V.1.0 version, the application of X-MP radar installed in Merapi Volcano, Indonesia, is developed as a soft-countermeasures of multimodal sediment disaster caused by eruption, which is historically one of the most active volcanoes in Indonesia. This attempt will complement the aforesaid utilization of radar technology and the forecasting model under the intelligent network as part of a unified flood management in volcanic basins.

## 2. Rainfall Remote Monitoring and Prediction by Radar

### 2.1. Technology of X-MP Radar

Weather radars transmit electromagnetic pulses toward the hydrometeors and measure the scattered signal. The measured parameter is echo intensity or reflectivity measured in dBZ. Radars are an appealing instrument for observing rainfall over large spatial domains within fine time resolutions. The X-MP radar is X-band radar, which is operated on a wavelength of 2.5-4 cm and a frequency of 8-12 GHz. With the short wavelength, the radar can provide higher resolution image of target identification. It provides rainfall measurement with 50 m spatial resolution and 2 minutes temporal resolution in real-time. X-band radars offer various advantages, including its capability to achieve fine spatial resolution and small size (Galgani et al., 2017) which is beneficial for hydrological purpose (Neto et al., 2018).

In contrast to conventional radars, which measure horizontal reflectivity ( $Z_H$ ), polarimetric radar measure from both horizontal and vertical polarizations ( $Z_V$ ). The fundamental polarimetric

parameters for estimating the rainfall intensity are differential reflectivity ( $Z_{DR}$ ) and specific differential phase ( $K_{DP}$ ) derived from differential propagation phase ( $\square_{DP}$ ) between vertical and horizontal polarizations. Since  $K_{DP}$  is less sensitive to raindrop size distribution variation (Maki *et al.*, 2005) and to attenuation by rainfall echo (Ryzhkov, *et al.*, 2005), quantitative rain estimates could be provided accurately (Scharfenberg *et al.*, 2005).

The radar hardware configuration consists of X-MP radar antenna unit connected with signal processing unit (SPU) which are placed outdoor and personal computer (PC) as indoor installation. The antenna uses solid-state transmitter which has higher durability than magnetron. LAN cables connect the transmit unit to SPU and to PC. The backscattered waves are processed by radio frequency converter and transferred to SPU. SPU processes the signals digitally and delivers them to the data storage unit through LAN cable. The data is stored in PC and displayed as images in real time. Bottom panel of Figure 1 shows the radar hardware configuration.

**2.2. Data Preprocessing Subsystem**

The radar parameters are obtained from constant altitude plan position indicator (CAPPI) scans. Jeong *et al.* (2014) used CAPPI data of radar to simulate runoff using SWAT model. CAPPI algorithm generates horizontal cross-section display of radar-observed parameters at specific layer height collected from all plan position indicator (PPI) scans. For hydrology purpose, CAPPI at the lowest elevation angle should be used if there are not beam blockages. Before being applied, attenuation of  $Z_H$  is corrected by using modified self-consistent method for X-band (Park *et al.*, 2005a).

$$10 \log_{10}[Z'_H(r)] = 10 \log_{10}[Z_H(r)] - 2 \int_0^r A_H(s) ds$$

$$A_H(r) = \frac{[Z'_H(r)]^b}{I(r_1, r_0) + (10^{0.1ba\lambda\phi_{DP}} - 1)I(r_1, r_0)}$$

where,  $Z'_H$  is attenuated  $Z_H$  ( $mm^6m^{-3}$ ),  $r$  is range,  $A_H$  is specific attenuation ( $dBkm^{-1}$ ),  $\square$  and  $b$  are coefficient and  $\square_{DP}$  is differential propagation phase ( $^{\circ}$ ). The coefficients are determined in accordance with optimal values for X-band (Park *et al.*, 2005b).

**2.3. Quantitative Precipitation Estimates**

Quantitative Precipitation Estimates (QPE) by weather radar is provided by the radar-rainfall algorithm. A composite method proposed by Park *et al.* (2005b) is adapted in this study:

$$(Z_H) = 7.07 \times 10^{-3} Z_H^{0.819} \text{ for } Z_H \leq 30dBZ \text{ or } K_{DP} \leq 0.3^{\circ}km^{-1}$$

$$R(K_{DP}) = 19.63K_{DP}^{0.823} \text{ otherwise}$$

where,  $K_{DP}$  is in  $^{\circ}km^{-1}$ ,  $R$  is in  $mm/h$  and  $Z_H$  is in  $mm^6m^{-3}$ . The results of this algorithm. After the preprocessing and radar-rainfall algorithm are applied, the radar-rainfall estimator product is obtained on  $50 \times 50$  m grid for 60 km range with for every observation time. Composite method is among the best quality of QPE products (Wang and Chandrasekar, 2010).

**2.4 Radar Echo Linear Extrapolation Model**

Prediction of near future rainfall helps to reduce the effect of rain-induced debris flow. This system is designed to enable the rainfall short-term prediction by using radar QPE in real-time scheme. Rainfall nowcasting systems currently use the extrapolation of observed radar reflectivity as the mainstream method (Mejsnar *et al.*, 2018). The nowcasting model used in this study is radar echo extrapolation model proposed by Shiiba *et al.* (1984). The dynamic of the horizontal rainfall intensity distribution  $r(x,y,t)$  with the spatial coordinate  $(x,y)$  at time  $t$  is described as follows:

$$\frac{\partial r}{\partial t} + m \frac{\partial r}{\partial x} + n \frac{\partial r}{\partial y} = w$$

$$m = \frac{\partial x}{\partial t}, n = \frac{\partial y}{\partial t}, w = \frac{\partial z}{\partial t}$$

where,  $m$  and  $n$  are advection vector by which the horizontal rainfall distribution is assumed to be translated, and  $w$  is the growth/decay rate of rainfall intensity. The  $m$ ,  $n$ , and  $w$  formations

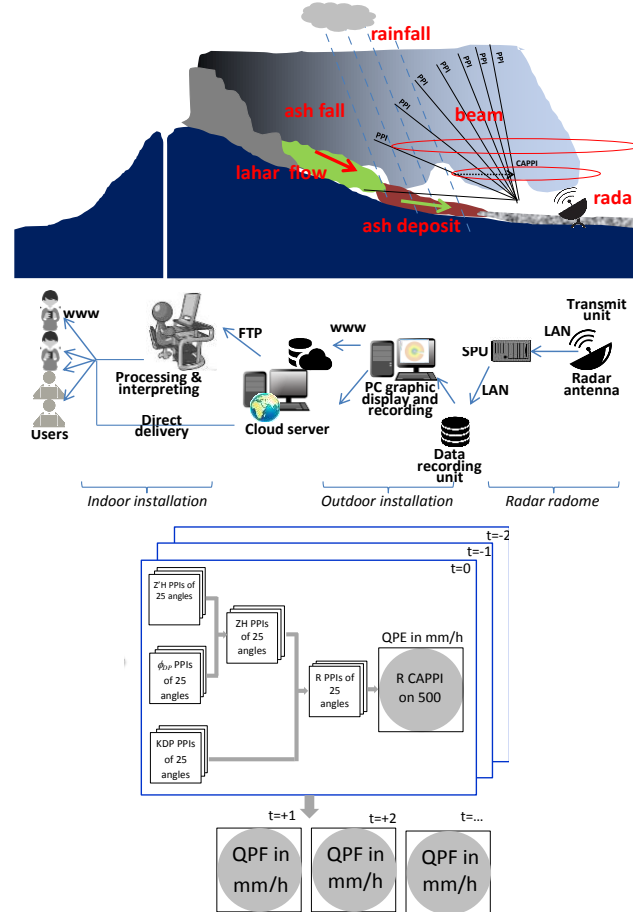


**Fig. 1:** QPE retrieval from radar observation and system infrastructure

are specified on each grid linearly in the manner of:

$$m(x, y) = c_1x + c_2y + c_3$$

$$n(x, y) = c_4x + c_5y + c_6$$

$$w(x, y) = c_7x + c_8y + c_9$$

The  $c_1$  to  $c_9$  parameters are optimized by linear least square using past observed radar-rainfall. This model is powerful for predicting short events within 3 hours lead time, yet the performance decreases rapidly for longer prediction time. The model predictability is verified by visually comparing the predicted and observed rainfall. As mentioned in Figure 1, the quantitative precipitation forecasts/QPF are modeled from the previously observed rain sheets produced every 2 minutes.

**2.5. Prediction of Debris Vulnerability Through Risk Mapping**

Previous studies stated that rain intensity and duration are important contributing factors to debris flow occurrence (Westen and Daag, 2005). In this research, the exceedance of rainfall to specific threshold is used to judge the risk level in grid basis using the predicted rainfall. Until recently, the debris flow early warning system primarily uses rainfall threshold (Pan *et al.*, 2018). Figure 2 shows the threshold line for debris in Boyong Rivers in one

control point from Mananoma and Wardoyo (2008) and black broken line from last five years observation.

To distinguish the river basin which is prone to debris, the prevalent rainfall based on the historical rainfall is analyzed along with slope parameter which also highly influences the debris flow event. Frequency analysis is employed to identify area with high likelihood of rainfall. From long recorded data, the area without high rain is marked with the lowest number. The area that is most frequently experiences high rain is marked with the highest number (Islam and Sado, 1999). Here, high rain refers to the threshold exceedance. The prevalence is shown by probability map showing the vulnerability score. The score is calculated as follows:

$$\text{Susceptibility score} = \text{Rank}_{\text{rain}} \cdot \text{Weight}_{\text{rain}} + \text{Rank}_{\text{slope}} \cdot \text{Weight}_{\text{slope}}$$

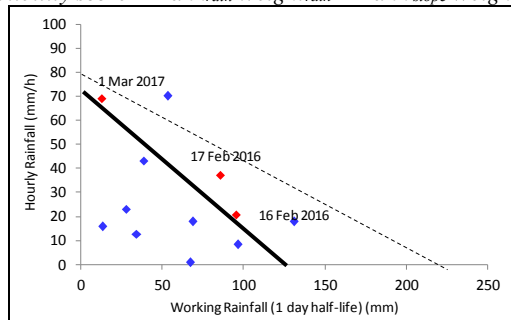


Fig. 2: Threshold of rain-induced debris occurrence in Boyong River

Same weights are assigned for both rain and slope factors. All parameter values are normalized from 0 to 1. The spatially distributed score is calculated by GIS technique and gives susceptibility index in grid basis. GIS has been used widely in flood disaster management in Vietnam (Tran et al., 2008) and America (Gunes and Kovel, 2000). In the case of sediment, La Ville et al. (2002) used remote sensing along with GIS, Chen and Yu applied GIS and morphometric analysis, and Di et al. (2008) employed GIS-based risk analysis of debris flow in Sichuan.

## 2 System Design of Risk Information

### 3.1 Framework of Rain-triggered Debris Disaster Information

A system for disaster mitigation through the application of X-MP radar in various types of water-related hazards is developed in this study. X-band Polarimetric Radar for Prevention of Water Disaster (X-Plore) is a platform of information system of rainfall monitoring and nowcasting observed by X-MP radar.

The implementation scheme X-Plore V.1.0 version including the design of its dissemination to the end-users is presented in Figure 3. The system provides two scheme of use, i.e. online, which is real-time application, and offline. Online data and calculations refer to the use of real-time data input and the analysis. The input data is radar-rainfall observation and debris threshold. The real-time QPE is displayed in rainfall spatial map all over the radar range in every two minutes by using the method explained in section 2.3. In order to see the progression of the rainfall rate in specific location as well as in targeted catchments, hyetograph is provided along with rain map. These graphs are updated with real-time data feed through the cloud and processing station.

The subsequent rainfall observations sheets are introduced to the rainfall prediction by radar echo extrapolation model. The method has been explained in section 2.4. Accordingly, the QPFs in rain map as well as in hyetograph can be shown in the system with two minutes interval. The risk map derived by using threshold in Figure 2 is also provided in this system. In other words, the outputs of online system are spatial rainfall observation, spatial rainfall prediction, hyetograph of rainfall observation, hyetograph of rainfall prediction, and risk map.

In this stage, the forecasting products are provided after some

period of time from the real-time. The lag is due to the time needed for data transfer and model running with sufficient spatial resolution. To handle single 6 hours prediction in single PC, 1 minute is required from data acquisition to analysis and interpretation.

As for the offline application, it provides disaster risk mapping based on predominant rain and slope gradient which is generated from the historical data of rainfall during observation campaign. The method is explained in section 2.5. This map can be utilized to identify basin and specific point that historically has high, which may lead to debris flow. In other words, the inputs of this system are past rainfall, debris threshold, and topographical map. The GIS analysis provides the long-term vulnerability map.

In the X-plore, only rainfall observation and debris susceptibility map can be accessed directly by the public. As for the forecasted

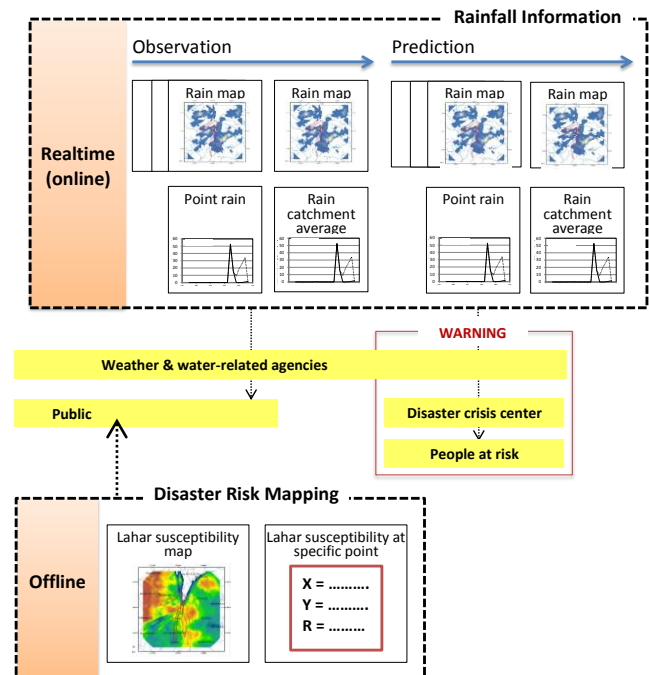


Fig. 3: Implementation plan of X-plore platform

rainfall, the information delivery should be interpreted by the water or weather-related authorities before being launched to the people at risk. In most countries, disaster warnings are issued by government. Careful use of prediction results is needed to avoid false alarm as well as failed detection as they may weaken public confidence.

The similar systems are found in Palau et al. (2018). It develops a model for forecasting areas that may be affected by debris flow in operational framework. However, it is applied over large scale instead of small scale rivers. In Hong Kong, the meteorological information system is developed by integrating spatial information that is able to store, manage, analyze, display and exploit geographic information (Wong, 2013).

### 3.2 GIS Web-based Platform

X-Plore platform is developed for providing geographical information system/GIS capabilities through maps that can be accessed from everywhere through web. The spatial rainfall intensity data is directly transferred in web map for whole observation domain. Through the GIS web-based platform, specific information is made available in flexible ways, such as rain intensity in every grid and rainfall distribution over the time.

The X-Plore webGIS is developed using Google API (Application Programming Interface). The API program code connects the Google Map to the web. At first, the maps API JavaScript code is added to the HTML. After getting the Google Maps API key, the map is set with the size of 120 x 120 km following X-MP radar range. Though the map extent is set to the maximum available data, the latitude and longitude are set to the coordinates of partic-

ular targeted river basins.

Google Fusion Tables provides the way to show the geographical data in Google Maps. The data from X-MP radar is uploaded in CSV format and geocoded according to the column with designated fields showing the location information. The CAPPI data product from X-MP radar has raster format with X, Y, Z value, showing the location of observed points and the value of the variable. Therefore, the CSV file is prepared based on point data and imported to Fusion Tables. The attributions of Z value placed in the columns consist of QPE, QPF, historical rainfall factor, slope factor, and susceptibility score with same spatial resolution. QPE and QPFAs there is limit of the total file size stored in the Fusion Table, the QPE and QPF data in real-time from the radar cloud server are introduced to Google Drive and updated each time the new data are supplied.

The website development uses CodeIgniter close source application. This is a framework for PHP server scripting language with Model, View, and Controller/MVC modeling for developing dynamic website. The small configuration of MVC architecture allows the simple website development for programmer and designer of X-Plore. The management system of rainfall spatial database on the web uses MySQL, which is run on server. The SQL statements are used to query and manipulate the fusion tables with HTTP requests. After all objects are ready, the browser will load the JavaScript Google Maps API using event onload command and the overlaid spatial data with Google Map can be seen in the X-plore website. A comparison with similar system is done. In Kong observatory, the system is developed by HTML5 web browser language, while the dynamic map is built by open source OpenLayers (Wong, 2013).

## 4 Use Case

### 4.1 Study Region

The study is conducted in river basins originated from Merapi volcano, Yogyakarta Special Province, Indonesia (7.5407°S, 110.4457°E) with elevation of 3317 AMSL as depicted in Figure 4. In the V.1.0 version, the application of X-MP radar installed in Merapi Museum (-7.616009, 110.424357) in January 2015 in the altitude of 755 AMSL, is developed for mitigation of multimodal sediment disaster caused by volcanic eruption. There are 12 rivers which are vulnerable for debris, e.g. Pabelan River, Boyong River, Putih River, Kuning River, Gendol River, Krasak River. As many as 70,000 people are living in the first danger zone over the Merapi flank. Observations of several rainfall occurrences in this area using X-MP Radar have shown that composite algorithm can estimate the rainfall intensity reasonably.

One significant eruption has occurred in October 2010. It has caused the debris flow in the subsequent rainy season. High amount of rain in March 2011 has brought 60% of volcanic material which was accumulated on the top. The debris flow was transported as far as 20 km with 110 km/hr speed of flow. In Gendol River, sediment reached 20 km and buried 21 houses, which evacuated 200 residents. X-MP radar was installed in January 2015 in Merapi Museum with the elevation of 755 MSL.

### 4.2. Online Web Application of GIS

In the Figure 5, the main menu of X-plore is shown. Figure 6 illustrates the observation results of X-MP radar on February 17, 2016 case in X-plore. The information about radar-rainfall intensity in particular point with X Y coordinate is shown in the comment balloon for 16.30 local standard time/LST. In order to see the progression of rainfall rate in specific location as well as in targeted catchments, hyetograph is provided together with precipitation mapping. The pink chart shows the CL and the black lines shows the real-time observed snake line development. This snake line will be an information to determine the initiation of the debris.

When the line approach the CL, an evacuation should be warned immediately.

It can be seen that the radar could capture the rainfall characteristic difference in terms of the magnitude as well as timing. Though Gendol River and Boyong River are near, the rainfall intensity of Gendol River was much higher than that of Boyong River. The maximum rain occurred with similar intensity but with short delay between neighbouring basins. It indicates that the radar could successfully capture the motion of the rain echo. It also shows the detail information of rainfall spatial distribution in hyetograph in X-Plore. The grid point rainfall intensity ranged from 1 mm/hr to 90 mm/hr. It can be seen by this menu, in average the rain over Gendol basin increased at 15.00 LST and reached the maximum at 16.15 LST with 3 hours total duration of heavy rain events, which is highly contributed to the occurrence of the debris disaster along the river stream.

Figure 7 demonstrates the menu of rainfall nowcasting up to 3 hours lead time. In order to evaluate the performance of

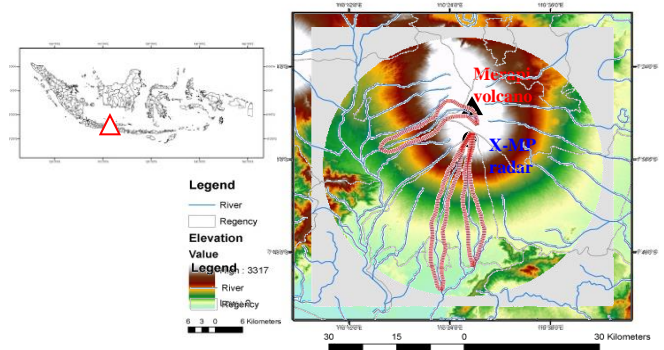


Fig. 4: Merapi volcano location, radar range, and rivers which are vulnerable for Merapi's debris (the catchments are indicated by red regions), topographical map

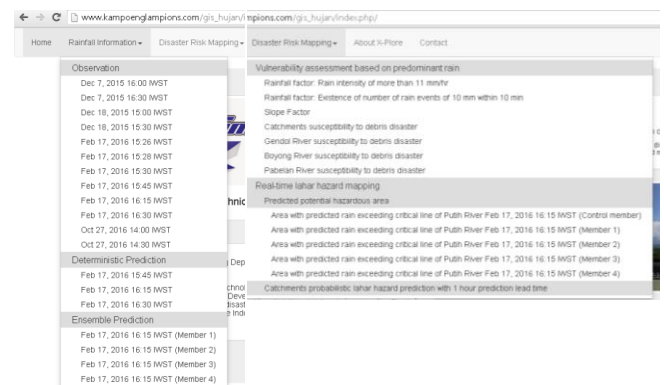


Fig. 5: X-plore home design

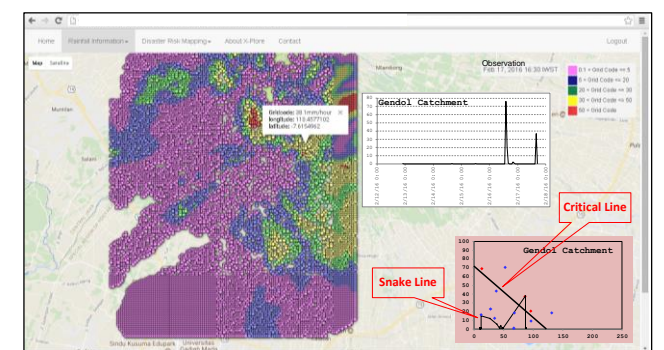


Fig. 6: Observed spatial QPE of February 17, 2016 case at 16.30 LST, hyetograph, and snake line at a specific point with X Y coordinate along with the critical line.

nowcasting model, the true radar echo pattern is displayed once the radar has completed the observation. Through the visual com-

parison, it is found that on some occasions the rain echo are in the incorrect position. This finding is in accordance with Mejsnar et al., (2018) who mentioned that the correlation for the extrapolation is 45.4 min. Generally, local convective storms are predicted poorly, while large-scale rainfall are better nowcasted. The predicted vulnerable area in one basin judged from the critical level exceedance is shown in hazard map as given in the inserted picture of Figure 8. This map would assist better decision making for the risk-prone region in emergency situation.

### 4.3 Offline Web GIS Implementation

The results of susceptibility map using past historical rainfall more than threshold are illustrated in Figure 9. The probability ranges from above 0 to nearly 1. Some areas have high probability of rainfall, such as around the summit of Merapi and above Progo River Magelang. This phenomenon may be attributable to orographic effect. Few regions experience two times of heavy rains that may induce debris flow and many places have one time heavy

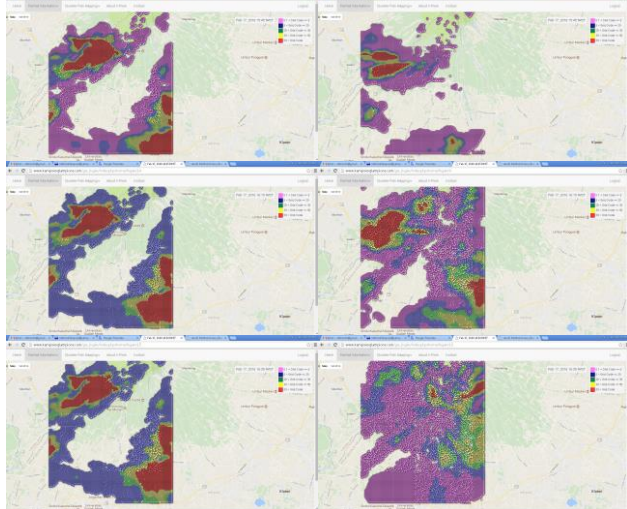


**Fig. 7:** Results of quantitative rainfall prediction of Gendol River disaster case for 15, 45, and 60 minutes lead time. The left panels are predictions and right panels are observations.

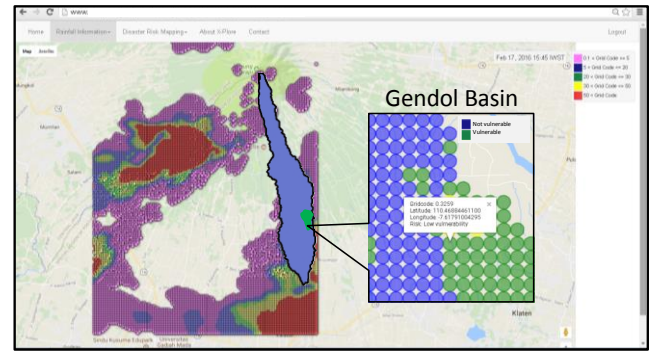
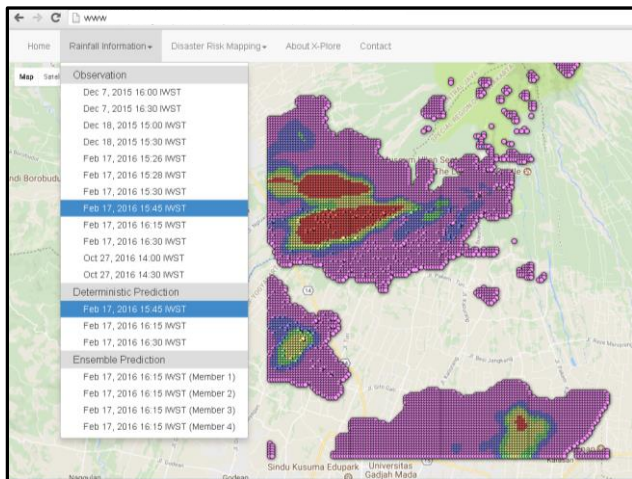


**Fig. 8** Quantitative rainfall prediction (mm/h) for 15 minutes lead time of February 17, 2016 case showing observation (left panel) and predictions with the hazard map in Gendol catchment (right panel) at 15.45 LST

rain from October 2015 to February 2016. From GDEM topographical data, slope of the terrain is calculated. The value is converted to absolute value as depicted in Figure 10. It can be inferred that 2 km surrounding the summit have the highest slope factor. This value will be combined with rain frequency factor to analyze the debris susceptibility in each region. Based on the probability of rain events selected from the debris threshold and slope factors, the susceptibility score is calculated spatially for each calculation grid by parametric method. Figure 11 provides the susceptibility of the catchments to the debris flow disaster drawn from data of observation campaign period. Red, yellow, and blue colors indicate the high, medium, and low susceptibility respectively. The past debris flood cases on Decem-

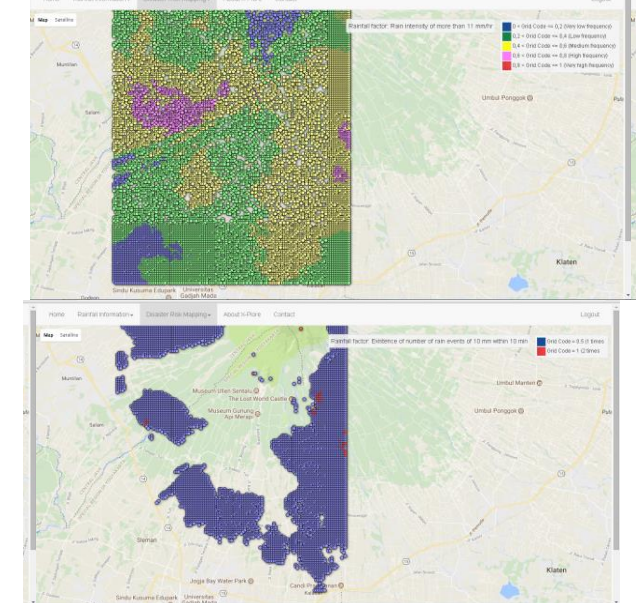


**Fig. 9:** Rain factors retrieved from observation campaign period

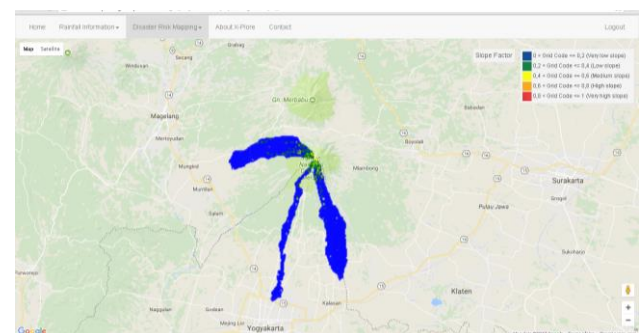


**Fig. 10:** Slope factor of Mount Merapi

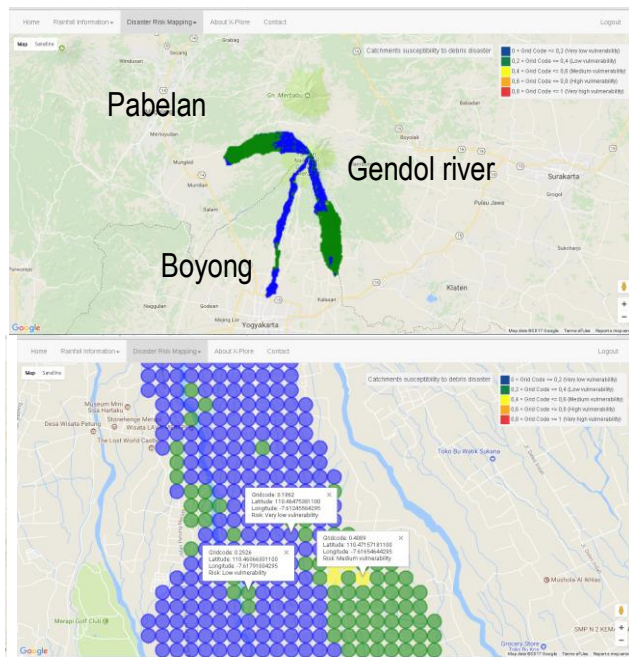


**Fig. 11:** Susceptibility of the catchments to the debris disaster from all observation data

ber 7, 2015, December 18, 2015, February 17, 2016, and October 27, 2016 have been reported that the debris flood occurred mostly Gendol Rivers. In addition, based on the disaster-prone mapping assessment by Geological Agency of Indonesia, Gendol River is included in the highest vulnerability level with wide range of prone area. The finding of the research is corroborated by the past observation, where Gendol River has middle to high vulnerability all over the catchment indicated by yellow-red color, particularly in 2 to 3 km from the top. According to Lavigne and Voight (2000), Gendol River is classified as second class of river that is most vulnerable to debris, after Putih River. Meanwhile, Pabelan and Boyong Rivers are categorized as third level. Yet, in this study, Putih River is not included in the analysis.

The prime motivation for communicating the forecast information like the above-mentioned scheme is to assist better decision making on the part of those receiving the information (Gill, 2008). By using the vulnerability map based on historical predominant rain, the detail information of the prone regions can be shown. The precipitation falls over certain small area can be distinguished with the neighboring area even in 100 m distant. The sparse available rain-gauges in the basins are not adequate to provide this information, which is significant for identifying the prone area.

## 5 Conclusion

This study has presented the use of the high-resolution X-MP radar for rainfall estimation and prediction which triggers the debris flow occurrence in volcanic region and the information system called X-plore. The rainfall prediction with lead time shorter than one hour gives promising degree of accuracy. Real-time snake line progression accessible through X-Plore web assists the decision making of warning and evacuation. The hazard map drawn from predicted rain and past predominant rain along with critical line shows the potential of X-MP radar utilization for deriving flood risk, despite much room for improvement. The proposed platform would be useful for communicating the disaster risk prediction based on weather radar in operational setting. The future study will be focused on system testing and the uncertainty assessment.

## Acknowledgement

This research was supported by the Science and Technology Partnership for Development, Japan Science and Technology Agency, and Japan International Cooperation Agency.

## References

- [1] Bradley DT, McFarland M & Clarke M (2014), The Effectiveness of Disaster Risk Communication: A Systematic Review of Intervention Studies. *PLoS Curr* 22(6).
- [2] Chen CV & Yu FC (2011), Morphometric analysis of debris flows and their source areas using GIS. *Geomorphology* 129, 387-397.
- [3] Di BF, Chen NS, Cui P, Li ZL, He YP & Gao YC (2008), GIS-based risk analysis of debris flow: an application in Sichuan, southwest China. *International Journal of Sediment Research* 23(2), 138-148.
- [4] Galgani G, Scozza G, Bolt RJ, Haider N (2017), Design and testing of a polarimetric X-band antenna for avionic weather radar. *Proceeding of European Microwave Conference*, 1167-1170.
- [5] Gill J (2008) *Guideline on Communicating Forecast Uncertainty*. World Meteorological Organization.
- [6] Gunes AE & Kovel JP (2000) Using GIS in Emergency Management Operations, *Journal of Urban Planning and Development* 126(3), 221-229.
- [7] Islam MM. & Sado K. (2000), Development of flood hazard map of Bangladesh using NOAA-AVHRR images with GIS. *Hydrological Sciences* 45(3), 337-401.
- [8] Jan M, Sokol Z, & Jana M (2018), Limits of precipitation nowcasting by extrapolation of radar reflectivity for warm season in Central Europe. *Nat. Hazards Earth Syst. Sci.* 18, 1395-1409.
- [9] Jeong C, Joo K, Lee W, Shin H, & Heo JH (2014). Estimation of optimal grid size for radar reflectivity using a SWAT model. *Journal of Hydro-Environment Research* 8(1), 20-31.
- [10] Kato A & Maki M (2009), Localized Heavy Rainfall Near Zoshigaya, Tokyo, Japan on 5 August 2008 Observed by X-band Polarimetric Radar: Preliminary Analysis. SOLA (2009), 89-92.
- [11] Mananoma T & Wardoyo W (2009) The influence of rainfall characteristics change on sediment migration pattern after Merapi eruption 2006. *Proceeding of International Seminar on Climate Change Impacts on Water Resources and Coastal Management in Developing Countries*, 1-10.
- [12] Maki M, Park SG & Bringi VN (2005), Effect of natural variations in rain drop size distributions on rain rate estimators of 3 cm wavelength polarimetric radar. *Journal of the Meteorological Society of Japan* 83(5), 871-893.
- [13] Mejsnar J, Sokol Z & Minarova J (2018) Limits of precipitation nowcasting by extrapolation of radar reflectivity for warm season in Central Europe. *Atmospheric Research* 213, 288-301.
- [14] Neary DG & Swift Jr LW (1987) Rainfall thresholds for triggering a debris avalanching event in the southern Appalachian Mountains, In: Costa, J.E., Wieczorek GF (ed) *Debris flow, avalanches: process, recognition, and mitigation*, GeolSoc Am Rev Engineering Geology (7), 81-92.
- [15] Neto ADL, Paz I, Borgez EC, Ichiba A, Tchiguirinskaia I & Schertzer D (2018), Hydrological responses to small scale rainfall variability over a semi-urban catchment using Multi-Hydro model: C-band vs. X-band radar data. *Geophysical Research* 20.
- [16] Palau RM, Berenguer M, Hürlimann M & Torres DS (2018), A prototype regional early warning system for shallow landslides and debris flows. *Geophysical Research* 20.
- [17] Pan HL, Jiang YJ, Wang J. & Ou GQ (2018), Rainfall threshold calculation for debris flow early warning in areas with scarcity of data, *Nat. Hazards Earth Syst. Sci.*, 18, 1395-1409.
- [18] Park SG, Bringi VN, Chandrasekar V, Maki M & Iwanami K (2005a) Correction of Radar Reflectivity and Differential Reflectivity for Rain Attenuation at X Band: Part I: Theoretical and Empirical Basis. *Journal of Atmospheric and Oceanic Technology* (22) 1621-1631.
- [19] Park SG., Maki M, Iwanami K, Bringi VN & Chandrasekar V (2005b) Correction of radar reflectivity and differential reflectivity for rain attenuation at X Band: Part II: Evaluation and application. *Journal of Atmospheric and Oceanic Technology* (22) 1633-1655.
- [20] Reyniers M (2008), Quantitative precipitation forecasts based on radar observations. Royal Meteorological Institute of Belgium.
- [21] Ryzhkov AV, Schuur TJ, Burgess DW & Heinselman PL (2005),

- The joint polarization experiment. *Bulletin of the American Meteorological Society* 86(1.6), 809-825.
- [22] Scharfenberg KA, Miller DJ, Schuur TJ & Schlatter PT (2005) The joint polarization experiment: Polarimetric radar in forecasting and warning decision making. *Weather and Forecasting* 20(5), 775-788.
- [23] Shiiba M, Takasao T, Nakakita E (1984) Investigation of short-term rainfall prediction method by a translation model, *Proceeding of Japan Conference on Hydraulic Engineering* (28) 423-428.
- [24] Tran P, Shaw R, Chantry G & Norton J. (2009), GIS and local knowledge in disaster management: a case study of flood risk mapping in Viet Nam. *Disasters* 33(1), 152-169.
- [25] Ville NDL, Diaz AC & Ramirez D (2002,) Remote Sensing and GIS Technologies as Tools to Support Sustainable Management of Areas Devastated by Landslides. *Geomorphology* 129(3-4), 387-397.
- [26] Wang Y & Chandrasekar V (2018), Quantitative precipitation estimation in the CASA X-band dual-polarization radar network. *Atmospheric Research* 213, 288-301.
- [27] Westen JV & Daag AS (2005), Analysing the relation between rainfall characteristics and lahar activity at Mount Pinatubo, Philippines. *Earth Surf. Process. Landforms*, 30.
- [28] Wong KW (2003) Development of Meteorological Information System Using Geographic Information System Technology, Hong Kong Observatory.